Engineering Structures 41 (2012) 199–208

Contents lists available at SciVerse ScienceDirect

Engineering Structures

journal homepage: www.elsevier.com/locate/engstruct

Buckling of anchored cylindrical shells of uniform thickness under wind load

Lei Chen [a,1], J. Michael Rotter [b,*]

[a] HeNan Electric Power Survey & Design Institute, Zheng Zhou, He Nan 450007, China
[b] Institute for Infrastructure and Environment, The University of Edinburgh, Edinburgh EH9 3JL, UK

ARTICLE INFO

Article history:
Received 23 June 2011
Revised 16 March 2012
Accepted 26 March 2012
Available online 26 April 2012

Keywords:
Cylindrical shells
Silos
Tanks
Uniform thickness
Wind pressure
Buckling

ABSTRACT

Cylindrical shells subjected to non-uniform wind pressure display different buckling behaviours from those of cylinders under uniform external pressure. At different aspect ratios, quite varied and complex buckling patterns occur: the results of linear and nonlinear buckling analysis can also be quite different. By contrast, cylinders under uniform external pressure always experience circumferential buckling and are little affected by changes in geometry, except in very short cylinders or changed boundary conditions.

This paper presents a wide-ranging study of anchored stocky and intermediate length cylindrical shells of uniform thickness under wind pressure. Its aim is to produce useful information for the design of silos and anchored tanks against buckling under wind. The finite element analyses indicate that both linear and nonlinear analyses predict the circumferential compression buckling mode in stocky cylinders. For intermediate cylinders, pre-buckling ovalization of the cross-section has an important influence on the buckling strength. Empirical expressions are developed to relate the linear and nonlinear critical stagnation pressures under wind to the classical critical value for uniform external pressure. The effects of yielding and imperfection sensitivity are also briefly explored.

1. Introduction

Thin-walled silos and tanks are in danger of buckling under wind when they are empty or only partially filled. These cylindrical shell structures display rather different buckling behaviours under non-uniform wind pressure from that under uniform external pressure. At different aspect ratios, quite varied and complex buckling patterns occur, and the predictions from linear and nonlinear buckling analyses can also be quite different. By contrast, cylinders under uniform external pressure always experience circumferential buckling and are relatively little affected by changes in geometry, except in very short cylinders or changed boundary conditions. The aim of this paper is to develop useful information for the practical design of silos and anchored tanks of all typical geometries against buckling under wind loads.

Cylinders under uniform external pressure have been extensively studied by many researchers and that literature is not reviewed here. The buckling of cylinders under wind has drawn significant attention only in more recent decades. Resinger and Greiner [1,2] produced design recommendations for the buckling of wind-loaded tanks based on the results of wind tunnel tests. They derived wind pressure distributions from their wind tunnel tests for both fixed-roof and floating-roof tanks with different geometric parameters. Ansourian [3] studied the elastic buckling of cylindrical shells under both uniform and non-uniform external pressure using the finite element method and found that his results agreed well with published analytical solutions for simpler cases. He also investigated the effect of an upper boundary ring stiffener on the buckling strength and deduced a criterion for the critical stiffness of this ring to enforce shell buckling without the ring's participation. Greiner and Derler [4] investigated the imperfection sensitivity of wind-loaded cylinders using numerical analyses, and examined several different imperfection shapes. They concluded that stocky shells are most sensitive to pre-buckling deformations in the form of the eigenmode, but longer shells are more sensitive to local imperfections in the form of a rectangular or ring shape. Later summaries put these studies into a wider context [5,6]. Pircher [7] continued this work exploring the buckling of medium-length cylinders under wind with a weld-induced axisymmetric imperfection. His focus was on the depth, shape and location of the imperfection so it did not extend to explore the effects of different shell geometries and thicknesses. Jaca et al. [8] used a lower bound approach to the buckling analysis of tanks subjected to wind pressures based on a reduced energy model. They showed that classical bifurcation buckling analyses provide an upper bound to both experimental and nonlinear computational results. Schneider and Zahlten [9] studied slender thicker cylinders ($h/r > 15$ and $r/t < 350$) relevant to chimney design using materially and geometrically nonlinear analyses under wind pressures, but

* Corresponding author. Tel.: +44 131 667 3576; fax: +44 131 650 6781.
E-mail addresses: chenleihe2008@yahoo.com.cn (L. Chen), m.rotter@ed.ac.uk (J.M. Rotter).
[1] Tel.: +86 15837190903.

0141-0296/$ - see front matter © 2012 Elsevier Ltd. All rights reserved.
http://dx.doi.org/10.1016/j.engstruct.2012.03.046

these are outside the scope of this study. None of the above produced a design method to cover the full range of geometries found in silos and anchored tanks.

The results of all these studies were known to the writers of the European Recommendations on Shell Buckling [10] when they produced a chapter [11] on the design of silos and tanks against buckling under wind loading. Although these recommendations give one clear design method for stocky cylinders and another for slender chimney-type cylinders, only a descriptive methodology is suggested for the intermediate range. This paper aims to address this shortcoming and to integrate the descriptions for stocky and intermediate cylinders so that the design process results in smooth changes between these categories.

In Chapter 12 of the European Recommendations on Shell Buckling [11], five different stability failure modes are identified in stocky, intermediate and slender cylinders respectively (Fig. 1). In stocky cylinders, the radial inward pressure in the stagnation zone induces compressive circumferential stresses that result in circumferential buckling modes similar to those in cylinders under uniform external pressure (Fig. 1a). In intermediate cylinders (Fig. 1b), the chief buckling mode is in the stagnation zone and is caused by the interaction of circumferential compression and axial compression generated by the external pressure, producing a buckle near mid-height on the windward generator, with a significant influence of geometric nonlinearity [4,5]. Alternatively, a shear buckle may form near the base (Fig. 1b). In slender cylinders (Fig. 1c), buckling may be caused by axial compression as for intermediate cylinders, or may occur by axial compression at approximately 90° from windward, or near the base of the shell in classic beam bending. It is clear that the buckling behaviour of cylinders under wind loading is quite complicated and involves many different modes for different geometries.

Most studies of wind-loaded cylinders have focused on tanks or silos of stocky shape (Fig. 1a) where the linear and nonlinear buckling modes are very close. The equations for buckling under wind given in ECCS EDR5 [10] are not differentiated in terms of the analysis used as their basis (linear or nonlinear). However, the philosophical framework of the European standard EN 1993-1-6 [12] indicates that the linear buckling pressure should be used as a reference measure to which the effects of geometric nonlinearity and imperfection sensitivity should be added later, so that process is followed here.

The boundary conditions of a shell can have a significant impact on its buckling resistance under external pressure [10,12], with the presence or absence of axial anchorage dominant in changing the resistance. Practical tanks and silos are never axially restrained at the top, so it is the base anchorage which is the key condition. As was well established by Schnell [13], anchorage at the base increases the buckling resistance under uniform external pressure by precisely 25%, and this condition is relevant to anchored tanks and effectively all silos. It is consequently the boundary condition used in this study.

Greiner [4] and Pircher [7] both showed that the linear and nonlinear buckling modes can be quite different in intermediate and long cylinders. Consequently, this paper explores the linear and nonlinear buckling predictions separately to obtain a better understanding of the relationship between the two and of the distinct effects of geometric nonlinearity. The effects of plasticity and imperfection sensitivity are also briefly presented. The analyses focus on silos and anchored tanks of practical geometry. Empirical expressions are developed to relate the linear and nonlinear critical stagnation pressures under wind to the classical critical value for uniform external pressure.

2. Wind pressures on cylindrical shells

Wind tunnel tests performed by Macdonald in the late 1980s [14,15] provided extensive quality wind data on silo structures with a range of aspect ratios. Rotter [16] used this data to devise a better pattern of wind pressures for a cylinder, which takes account of the changing circumferential pattern as the aspect ratio varies. This description was adopted into EN 1993-4-1 Annex C [17]. For an isolated cylinder with a closed roof, the circumferential variation of the pressure (positive inward) may be expressed as [17]:

$$C_P = -0.54 + 0.16(d_c/L) + \{0.28 + 0.04(d_c/L)\}\cos\theta + \{1.04 - 0.20(d_c/L)\}\cos 2\theta + \{0.36 - 0.05(d_c/L)\}\cos 3\theta - \{0.14 - 0.05(d_c/L)\}\cos 4\theta \quad (1)$$

where θ is the circumferential coordinate from windward, d_c is the diameter of the cylinder and L is the overall height of the complete structure (the cylinders studied here are all ground-supported). For cylinders with L/dc less than 0.50, the value of C_p for $L/d_c = 0.50$ should be adopted [17].

Eq. (1) is the only known expression for the wind distribution that considers the significant effect of the aspect ratio of the structure. This paper focuses on isolated cylinders, so Eq. (1) was adopted throughout the study. As in most previous studies, the wind pressure is assumed to be invariant up the height of the shell. The circumferential variation of the wind pressure given by Eq. (1) at different aspect ratios is shown in Fig. 2, where the strong effect of aspect ratio is clear, especially in short cylinders. Clearly, slight changes in the ratio of length L to radius r may significantly change the wind pressure distribution. However, for intermediate and

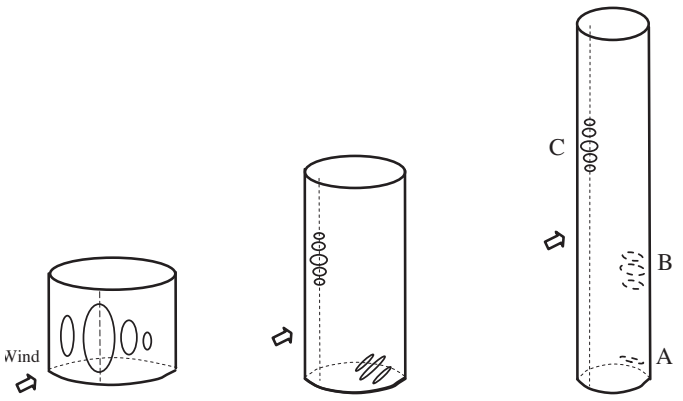

Fig. 1. Buckling modes in cylinders of different aspect ratio under wind [10]. (a) Stocky cylinder, (b) Intermediate cylinder, (c) slender cylinder.

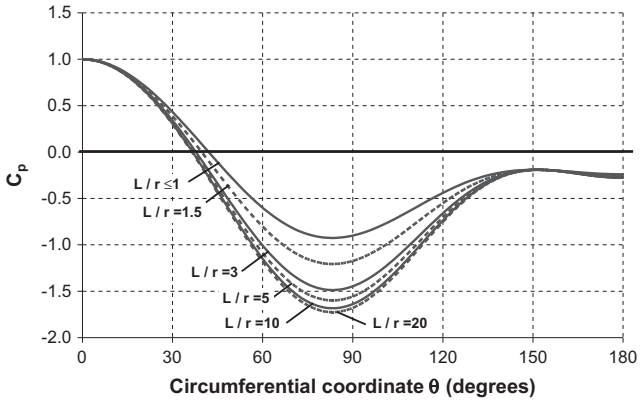

Fig. 2. Wind distribution coefficient around the circumference for cylindrical shells with different L/r according to EN 1993-4-1 [17] ($r/t = 500$).

slender cylinders, the wind distribution naturally changes little as the length is increased.

3. Scope of the calculations

The buckling behavior of silos and anchored tanks of practical geometry under wind pressure was studied using the finite element program ABAQUS [18]. Silo aspect ratios are generally in the range ($0.5 < L/r < 8$ with $200 < r/t < 1000$) where t is the wall thickness of any strake. Tanks are often squatter and thinner ($0.1 < L/r < 4$ with $500 < r/t < 2000$). Some geometries slightly outside the above ranges were also included here for completeness. The shell was made of an elastic isotropic material with Young's modulus $E = 2.0 \times 10^5$ MPa and Poisson's ratio $v = 0.3$. However, the results are all presented in a dimensionless form so that they can be applied to any metal shell. In the calculations that included material plasticity, an ideal elastic–plastic model was adopted with von Mises criterion and a yield stress $\sigma_y = 250$ MPa. A ring stiffener with sufficient flexural stiffness according to the rule in ECCS EDR5 [10] was used at the top boundary to limit the ovalization of the cross-section under wind to 2% [19]. At the base, all translations were restrained but the meridional rotation was left free. It may be noted that many oil tanks are not axially restrained at the base, and this study does not address this case. However, it may also be noted that whenever the buckling mode does not extend to the base in a stepped wall silo, the base of the buckle is effectively anchored [20]. The wind pressure pattern was characterised by Eq. (1) with a unit value for the stagnation pressure q_{stag} that was deemed invariant with height.

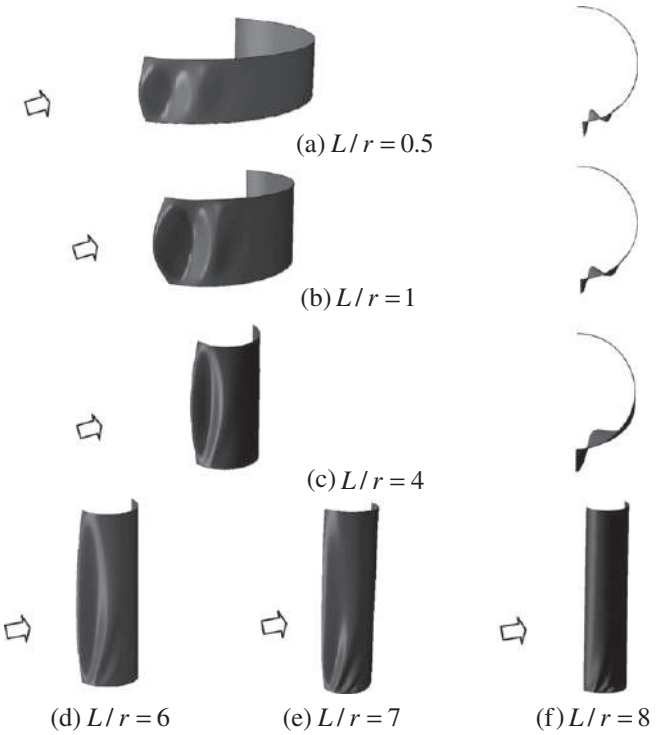

Fig. 3. Linear critical buckling modes for cylinders under wind pressure with changing length to radius ratios ($r/t = 200$).

4. Linear elastic bifurcation in cylinders under wind pressure

4.1. Introduction

In general, the result of a linear bifurcation analysis (LBA) cannot be justified as a reliable strength assessment for a practical shell structure because the true strength may be quite sensitive to geometric nonlinearity and geometric imperfections, which are both ignored in linear bifurcation analyses (LBA) [21]. However, LBA analysis determines the elastic critical buckling resistance, which is a key reference value for all shell buckling analyses, since it gives the first estimate of the elastic buckling strength, is unique, is always calculable when compressive stresses occur in the structure, and can usually be represented by a relatively simple equation following a parametric numerical study [21,22]. For these reasons, it is adopted as the elastic reference failure strength in EN 1993-1-6 [12] to be modified approximately to account for the more complex effects of imperfections and plasticity.

4.2. Linear elastic buckling mode for cylinders with r/t = 200

The linear buckling behaviour under wind was investigated first for cylinders with thickness $r/t = 200$ and lengths in the range $0.5 \leqslant L/r \leqslant 8$. The linear buckling modes for different length to radius ratios are shown in Fig. 3.

When L/r is small, as shown in Fig. 3a–c for $L/r = 0.5$, 1 and 4 respectively, the linear buckling mode is similar to the classical circumferential compression mode (Fig. 1a). When L/r increases to $L/r = 6$ and 7 (Fig. 3d and e), the critical mode changes. As will be described in detail in Section 4.4, compressive axial membrane stresses are induced by the unsymmetrical pressure on the shell, comparable with those found with other cases involving strips of inward pressure on cylindrical shells [23]. This axial compression produces a main long buckle on the windward meridian extending over almost the whole height, accompanied by smaller fold-like buckles towards the base. This buckling mode was not identified in Fig. 1, taken from [10]. When $L/r = 8$ (Fig. 3f), the mode changes to a local shear buckling mode with several small fold-like buckles near the base of the side meridian (90°) extending over a limited zone of the shell. The pre-buckling stress patterns are explained in the context of these mode changes in Section 4.4.

4.3. Linear elastic buckling stagnation pressures for cylinders with r/t=200

To introduce the linear bifurcation behaviour of shells of different aspect ratios, analyses were first performed on cylinders with a fixed radius to thickness ratio $r/t = 200$. The stagnation pressures at buckling $q_{cr,LBA}$ were evaluated relative to the buckling uniform pressure determined from Donnell theory for intermediate length cylinders with simply-supported edges [24,25] and free to displace axially at the end boundaries:

$$q_{cr,D} = 0.92E\left(\frac{t}{r}\right)\left(\frac{\sqrt{rt}}{\ell}\right) \tag{2}$$

in which ℓ is the half wave-height of the buckle, which is equal to the whole height L for a cylinder of uniform thickness. The corresponding finite element calculation for uniform external pressure was also performed for comparison purposes, and these show the differences between the true uniform buckling pressure and the reference Donnell value.

The buckling pressure ratios $q_{cr,LBA}/q_{cr,D}$ are shown for both uniform external pressure and wind in Fig. 4, where the wind pressure distribution is characterised by the stagnation value. The restraint of axial displacements at the base accounts for a notional 25% increase in the buckling pressure under uniform external pressure [10,12,13], and is clearly visible at larger L/r ratios. The wind stagnation pressure at buckling is generally much larger than the uniform external pressure value.

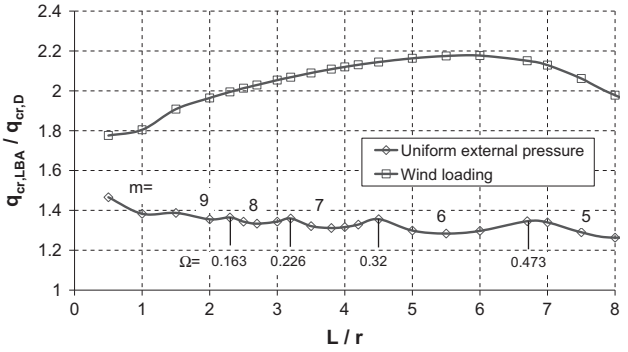

Fig. 4. Linear bifurcation pressures under wind and uniform external pressure ($r/t = 200$).

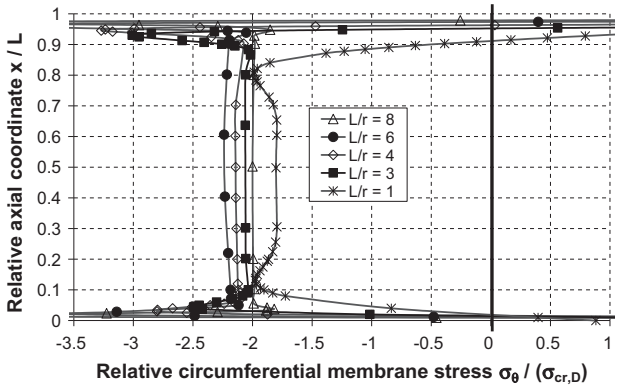

Fig. 5. Circumferential membrane stress distribution up the windward generator ($r/t = 200$).

Under uniform external pressure, the relationship between critical pressure and length has several cusps, which correspond to progressive changes in the buckling wave number around the circumference (Fig. 4). These cusp points are identified in terms of the dimensionless parameter Ω, which is defined later, but is marked here so that a connection can be made with the later description. By contrast, under wind pressure, the dimensionless stagnation buckling pressure ratio $q_{cr,LBA}/q_{cr,D}$ increases smoothly with increasing L/r in the range $0.5 \leqslant L/r \leqslant 6$ but decreases again beyond $L/r = 6$ as the pre-buckling stress distribution and resulting linear buckling mode changes. These changes are described below.

4.4. Membrane stress distribution derived from linear elastic analysis

To understand the changes in buckling strength under wind, it is useful to examine membrane stress distributions at the critical stagnation pressure. The linear critical pressure distribution derived from each linear bifurcation analysis (LBA) was applied to each shell. The distributions of circumferential and axial membrane stress (tensile positive) up the windward generator are shown in Figs 5 and 6 and that of the axial membrane stress around the base in Fig. 7. The circumferential membrane stress was made dimensionless using the Donnell value $\sigma_{cr,D} = (r/t)q_{cr,D}$ and the axial stress relative to the classical elastic critical stress for a uniformly compressed cylinder [10]. The vertical coordinate x is normalized by the cylinder height as x/L with $x = 0$ at the base.

When the cylinder is short ($L/r = 1$), the compressive axial membrane stress on the windward meridian is tiny (Fig. 6), but the circumferential membrane stress is nearly double that for uniform external pressure (Fig. 5) because of the circumferential pressure variation within the buckle (cf. Fig. 4). The result is a circumferential buckle (Fig. 3b). The compressive axial membrane stress near the base at 80° from windward (Fig. 7) is far smaller than the classical value and the boundary restraint prevents buckling.

At larger values of L/r ($3 \leqslant L/r \leqslant 6$), compressive axial membrane stresses grow significantly in the upper half of the cylinder with a peak around $x/L = 0.62$ (Fig. 6), but the stagnation circumferential membrane stress on the windward generator still rises (Figs 4 and 5) as the critical buckle grows in size (Fig. 3c) and encompasses more of the circumferentially reducing pressure pattern (Fig. 2). But at greater aspect ratios ($L/r \geqslant 6$), the axial membrane stresses at around $x/L = 0.62$ (Fig. 6) begin to play a very strong role, and the growing values around $\theta = 80°$ at the base begin to change the buckle form (Fig. 3d–f), both leading to reduced critical stagnation pressures (Fig. 4). This phenomenon was previously noted by Resinger and Greiner [2].

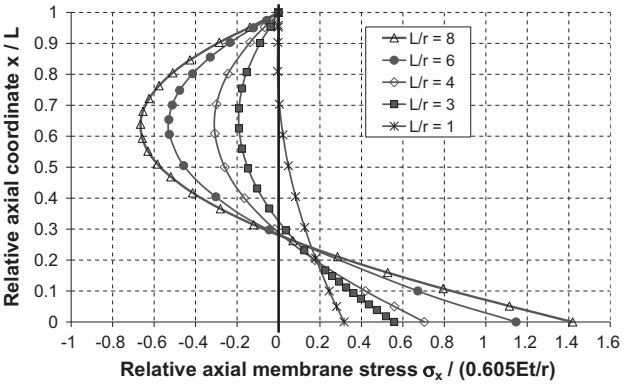

Fig. 6. Axial membrane stress distribution up the windward generator ($r/t = 200$).

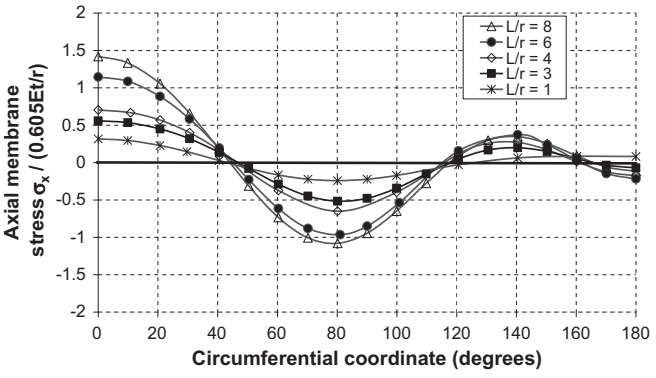

Fig. 7. Axial membrane stress distribution around the circumference at the base ($r/t = 200$).

The dimensionless radial displacement on the windward generator under the corresponding linear critical buckling stagnation pressure $q_{cr,LBA}$ is shown in Fig. 8, with inward displacements positive. At the top, the upper boundary translates as a rigid body, with values that naturally grow as the length increases. However, the pattern of these shell displacements is nothing like a cantilever because local shell deformations totally dominate. In cylinders with $L/r \geqslant 3$, the maximum radial displacement occurs at around $x/L = 0.62$, which is the same as the location of the maximum compressive axial membrane stress (Fig. 6). It is later seen that these large pre-buckling deformations influence the nonlinear buckling mode and pressure significantly.

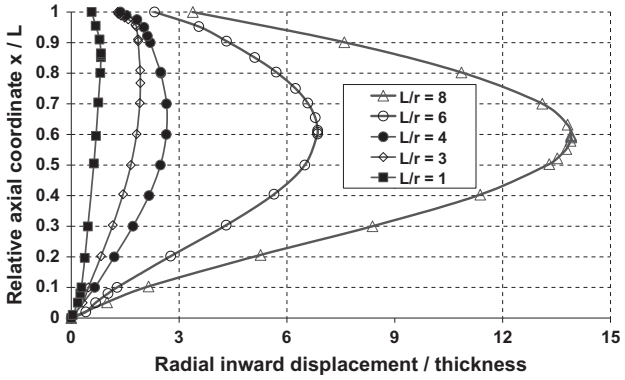

Fig. 8. Radial prebuckling displacement at windward at the linear critical pressure ($r/t = 200$).

4.5. Relationship of the linear elastic buckling pressures for cylinders under wind pressure and uniform external pressure

It is natural to try to relate the linear buckling wind stagnation pressure to that under uniform pressure [1,2,10,12]. Here, the critical value under uniform external pressure is written $q_{u,LBA}$ and that for the wind stagnation pressure as $q_{w,LBA}$. The relationship between the buckling pressure ratio $q_{w,LBA}/q_{u,LBA}$ and the shell length parameter Ω is shown in Fig. 9 for four values of the radius to thickness ratio r/t. The curves for different values of r/t are very similar if the length is described in terms of the dimensionless parameter Ω:

$$\Omega = (L/r)(t/r)^{1/2} \tag{3}$$

The uniform external buckling pressures $q_{u,LBA}$ in Fig. 9 were determined from finite element calculations and are similar to those defined by the algebraic expressions in EN 1993-1-6 [12] but exceed them by between −1% and +8%. These discrepancies are attributable to the requirement that design standards present conservative estimates that ignore the cusping associated with changes in the buckling mode.

The value of $q_{w,LBA}/q_{u,LBA}$ in Fig. 9 is always larger than unity, indicating that the stagnation pressure at buckling is always greater than the uniform external pressure buckling value. When the shell is very short, this ratio is close to unity, because the half wavelength of a buckle in the stagnation zone is very short and the pressure is almost uniform within each buckle, so the response on the windward generator is similar to that for uniform external pressure. This effect was noted by Brendel et al. [26].

As the size of the critical uniform pressure buckle grows with increasing aspect ratio, the wind pressure varies more significantly within it, causing a steady increase in $q_{w,LBA}/q_{u,LBA}$ until a maximum

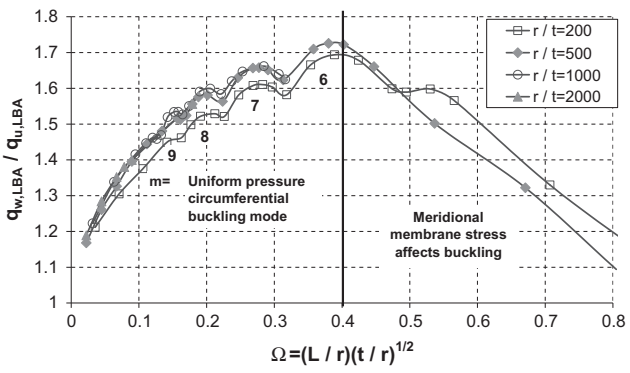

Fig. 9. Linear wind bifurcation pressure ratio $q_{w,LBA}/q_{u,LBA}$ and length parameter Ω.

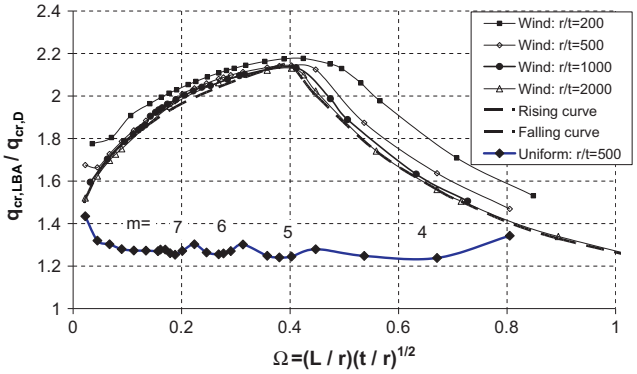

Fig. 10. Linear wind bifurcation pressure ratio $q_{w,LBA}/q_{cr,D}$ and length parameter Ω.

value around 1.70 is reached at $\Omega = 0.4$. Beyond this maximum (Fig. 9), the value of $q_{w,LBA}/q_{u,LBA}$ steadily decreases with a further increase of Ω, due to the significantly increasing axial membrane stress, as noted above.

The chief difficulty in relating the wind buckling pressure to the uniform external buckling pressure is shown clearly when comparing Figs 4 and 9. Under wind, the buckling pressure varies smoothly with cylinder length (Fig. 4), but cusping occurs under uniform external pressure, so that a neat empirical relationship to capture the data in Fig. 9 must always be conservative and loses accuracy. If instead, the data in Fig. 9 is shown relative to the Donnell pressure (Eq. (2)), the result of Fig. 10 emerges, where the two phases of behaviour under wind become quite distinct.

The curves for all radius to thickness ratios now all fall in much the same place, with the thicker $r/t = 200$ line some 4–5% above the rest for $\Omega < 0.4$ and 12% above at larger Ω.

Approximate expressions can now be chosen to represent both the rising part (stocky cylinders) and the falling part (intermediate cylinders) of the curves in Fig. 10. The rising part is closely represented by

$$q_{w,LBA}/q_{cr,D} = 0.83 + 1.64\Omega^{0.23} \quad \Omega \leqslant 0.40 \tag{4}$$

and the falling part by

$$q_{w,LBA}/q_{cr,D} = 0.55 + 0.705\Omega^{-0.9} \quad 0.40 < \Omega \leq 1.4 \tag{5}$$

with the new boundary between stocky and intermediate lengths identified by $\Omega = 0.40$ at which point these two expressions match. Eq. (5) has been verified for values of Ω to 1.40, beyond which the value of $q_{w,LBA}/q_{cr,D}$ reaches a plateau at a value of 1.07.

Eqs. (4) and (5) fit the accurate numerical predictions very well, providing lower bounds to calculations (Fig. 10) for all practical r/t ratios. For all but the thicker cylinders ($r/t = 200$), Eq. (4) slightly underestimates the precise values (<3%), whilst the accuracy of Eq. (5) depends more on r/t, but is closer than 3% for $r/t \geqslant 1000$.

Eq. (4) is valid for stocky cylinders with lengths in the range $0 < \Omega \leqslant 0.40$, for which the circumferential compression buckling mode is critical. The upper limit of $\Omega = 0.40$ corresponds to different values of L/r for different values of r/t as shown in Fig. 11. A comparison of this limit with typical geometries of silos, tanks, chimneys and wind generator towers shows that most silos and tanks are covered by Eq. (4) whilst most chimneys are not.

5. Geometrically nonlinear analysis of cylinders under wind pressure

5.1. Introduction

Two types of buckling occur in shells [10]: bifurcation or snap-through buckling. The LBA prediction covers only bifurcation

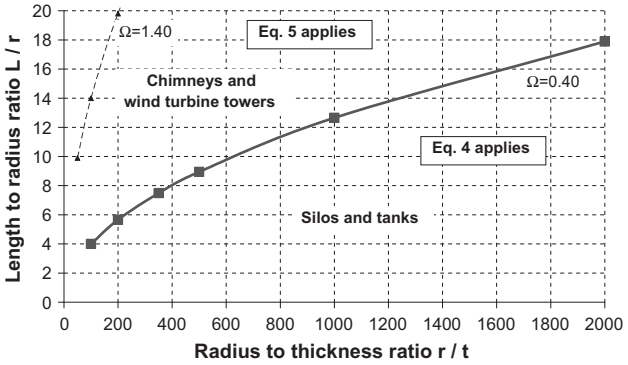

Fig. 11. Limits of validity of Eqs. (4) and (5) for different r/t based on LBA analyses.

buckling with no change of geometry [10]. For cylinders under uniform external pressure, the load–deflection curves for geometrically nonlinear analysis are close to linear in the pre-buckling range, the pre-buckling deformations are small and have only a small influence on the buckling behaviour, which cause the critical buckling pressure under LBA and GNA analyses to be very similar [27,28]. However, geometric nonlinearity can be significant for some cylinders under wind loading [3–7,9,19]. Large deformations can change both the pre-buckling stress distribution and the susceptibility of the modified geometry to buckling. The nonlinear buckling pressure can consequently be much smaller than the linear critical pressure. The nonlinear buckling mode may also be quite different from the linear buckling mode. Thus geometrically nonlinear analysis (GNA) is needed to obtain satisfactory buckling strength predictions for cylinders under wind pressure.

5.2. Geometrically nonlinear analysis for cylinders with $r/t = 200$

The nonlinear buckling behaviour for wind-loaded cylinders with lengths in the range $0.5 \leqslant L/r \leqslant 8$ is here initially described for a fixed $r/t = 200$. Using the maximum radial displacement up the windward generator to characterise the deformations, the nonlinear stagnation pressure–displacement curves are shown in Fig. 12 for a few sample geometries. The stagnation pressure was normalized by the linear critical value $q_{w,LBA}$ for each case.

For stocky cylinders with $L/r \leqslant 3$, snap-through buckling occurs and a bifurcation point appears just after this limit load has been reached. Pre-buckling deformations are small before the limit load is reached. The nonlinear buckling pressure is close to the linear elastic critical pressure, indicating that geometric nonlinearity has little effect on the buckling strength, as for uniform external pressure. The nonlinear mode is the circumferential compression buckling mode as shown in Fig. 13a and b for $L/r = 1$ and $L/r = 3$.

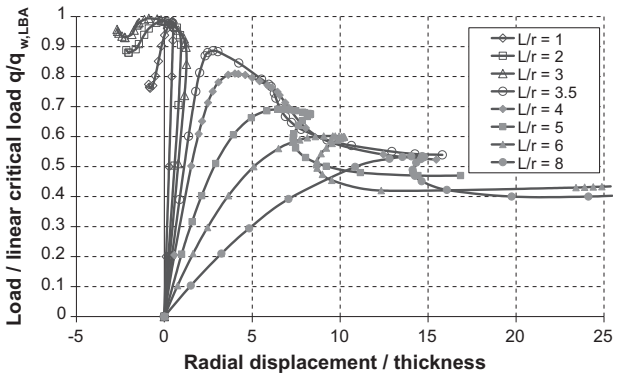

Fig. 12. Maximum radial displacement on the windward meridian ($r/t = 200$).

After the limit point, the outward radial displacement increases under decreasing load.

For cylinders of higher aspect ratio, the load–displacement curves display rather different behaviours depending on the specific value of L/r. When $L/r = 3.5$ or 4, the radial inward deformations remain quite small and the curves are quite linear until shortly before the limit point. This buckle has a long wavelength axially and occurs over a large zone in the upper part of the windward meridian, caused by the interaction of axial compression and circumferential compression (the nonlinear buckling mode at the limit point in Fig. 13c and d). The snap-through buckling pressure ratio $q_{w,GNA}/q_{w,LBA}$ falls steadily as L/r increases, where $q_{w,GNA}$ is the nonlinear buckling stagnation pressure under wind.

After snap-through, the pressure decreases quickly, with accelerated inward radial deformation until a bifurcation occurs, leading to a more dramatic fall in strength and decreasing radial displacements under decreasing pressures. The bifurcation produces a local short wavelength buckle with a maximum inward displacement at about $x/L = 0.62$ (bifurcation buckling mode in Fig. 13d). The location of this bifurcation buckle corresponds to the linear analysis maximum compressive axial membrane stress (Fig. 6). This local bifurcation buckle is caused by a significant pre-buckling flattening of the shell coupling with these axial stresses. Similar small bifurcation buckles in considerably deformed shells under non-symmetric loads can be seen in studies of other load cases [29,30].

As the cylinder length increases further ($L/r > 4$), the pre-buckling path become more nonlinear (Fig. 12), with stronger pre-buckling flattening on the windward generator, leading to a more significant reduction in the axial buckling resistance. Bifurcation with a more dramatic post-buckling fall follows the limit point.

If the cylinder is long enough ($L/r \geqslant 6$), bifurcation precedes the snap-through (Figs. 12 and 13f). For these cylinders, bifurcation involving small wavelength axial buckles controls the strength and the nonlinear buckling pressure is much lower than the linear critical pressure.

5.3. Comparison of the linear critical and nonlinear buckling pressures for cylinders under wind pressure

The effect of geometrically nonlinearity under wind is best seen by examining the ratio of the geometrically nonlinear wind buckling pressure $q_{w,GNA}$ to the linear bifurcation wind pressure $q_{w,LBA}$. The ratio of these pressures $q_{w,GNA}/q_{w,LBA}$ is plotted against a new length parameter ξ (Eq. (6)) for cylinders with different radius to thickness ratios in Fig. 14. The curves for different values of r/t can be seen to be very similar if the length is described in terms of the alternative dimensionless length parameter ξ:

$$\xi = (L/r)(t/r)^{4/7} \tag{6}$$

For stocky cylinders with lengths in the range $0 < \xi \leqslant 0.16$, the value of $q_{w,GNA}/q_{w,LBA}$ is stable and close to unity. For intermediate cylinders ($0.16 < \xi \leqslant 0.34$), pre-buckling deformations quite abruptly have a detrimental effect on the buckling strength, causing a considerable reduction in the buckling pressure for relatively small changes in geometry. The reduction grows as the length increases further but finally stabilizes towards an asymptotic value of 0.53. For thinner cylinders, the asymptotic value may be slightly higher than 0.53 (~5% higher for $r/t = 500$ and ~10% higher for $r/t = 1000$).

The relationship between the buckling pressure ratio $q_{w,GNA}/q_{w,LBA}$ and the length parameter ξ in the range $0.161 < \xi \leqslant 0.344$ can be closely empirically approximated by:

$$q_{w,GNA}/q_{w,LBA} = \frac{0.1}{2.12\xi^{0.06} - 1.8} \tag{7}$$

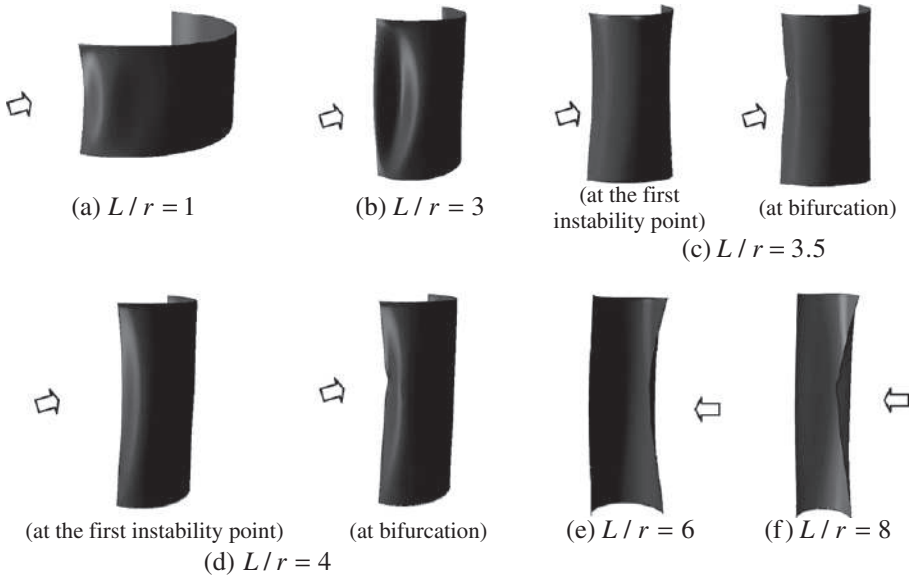

Fig. 13. Nonlinear buckling modes for cylinders under wind pressure (r/t = 200).

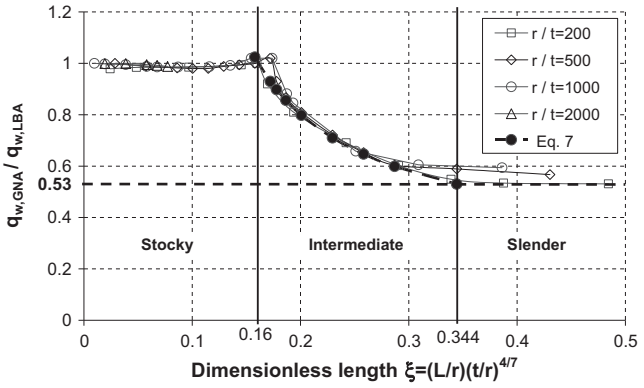

Fig. 14. Relationship between geometrically nonlinear and linear bifurcation pressures.

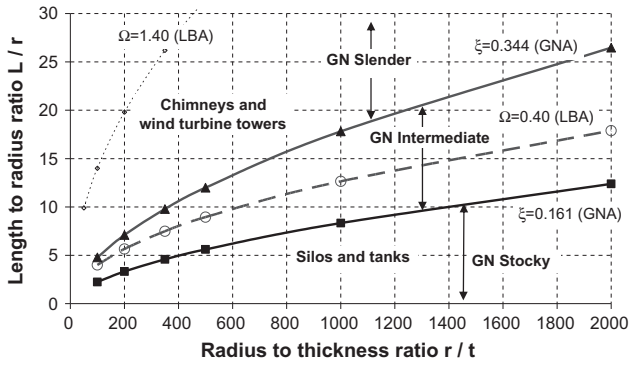

Fig. 15. Boundaries between stocky, intermediate and slender cylinders under GNA and LBA analyses.

The dashed line representing Eq. (7) in Fig. 14 fits the numerical results for different values of r/t very well. The relationship between the geometrically nonlinear buckling strength and the linear bifurcation value can thus be captured well with three domains, two with the fixed ratios $q_{w,GNA}/q_{w,LBA}$ = 1.0 and 0.53, and the intervening zone covered by Eq. (7).

It is interesting to note that the boundaries between different behaviours in the linear bifurcation analysis and those that transform the linear to the nonlinear result are different and depend on different dimensionless length parameters (albeit similar). As a result, it is probably not a good idea to try to produce a design method that achieves the geometrically nonlinear analysis outcome in a single step. Instead it seems better to separate these two aspects, as is done in EN 1993-1-6 [12].

Since there are different boundaries for the categories of stocky, intermediate and slender cylinders in Figs. 10 and 14, it is useful to re-draw Fig. 11 with this fuller set of information. The result is shown in Fig. 15 where the boundaries of L/r and r/t values between stocky, intermediate and slender cylinders based on GNA analyses are contrasted with those for LBA analyses. It is clear that the class of stocky cylinders becomes more restricted when geometrically nonlinear effects are included.

6. Geometrically and materially nonlinear analysis

In some shell structures, the buckling behaviour can change dramatically when a relatively small region begins to yield [31]. For thin cylinders under wind pressure, plasticity only affects the buckling strength of comparatively thick cylinders, and these may not be very susceptible to buckling anyway. The relationship between the buckling pressure ratio under potentially plastic conditions $q_{w,GMNA}/q_{w,LBA}$, together with that for elastic behaviour $q_{w,GNA}/q_{w,LBA}$, is shown in Fig. 16 for two values of radius to thickness ratio.

A comparison of these two analyses gives a direct measure of the global effect of plasticity. For thinner cylinders with r/t = 500, the analysis including plasticity (GMNA) and the elastic analysis (GNA) are identical for all values of Ω (Fig. 16), indicating that plasticity has no macroscopic effect on the buckling behaviour.

In the thicker cylinders with r/t = 200, plasticity reduces the buckling strength (Fig. 16) as yield occurs in different places depending on the value of L/r. In stocky cylinders, a zone near the base away from the windward (Fig. 17a–c) locally yields under high membrane stresses (Figs. 6 and 7). At greater lengths (Fig. 17d–f), yielding at the base of the windward generator occurs under axial tensile membrane stresses before buckling.

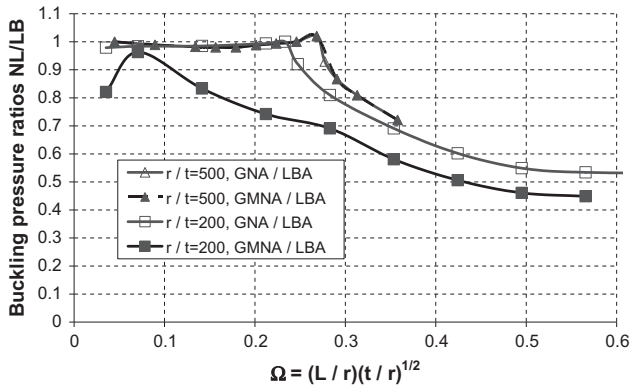

Fig. 16. Buckling pressure ratios for elastic nonlinear $q_{w,GNA}/q_{w,LBA}$ and elastic–plastic nonlinear $q_{w,GMNA}/q_{w,LBA}$ analyses.

It may be concluded that plasticity does not play a significant role in the wind buckling behaviour of cylinders with $r/t \geqslant 500$, but is clearly important in chimneys and wind turbine towers [9,19,32].

7. The effect of geometric imperfections

7.1. The pattern and amplitude of assumed geometric imperfections

Whilst shells are notoriously sensitive to minor geometric imperfections, the loss of buckling strength under external pressure is often less significant than for other conditions [28]. Under wind loading, the localisation of the stresses suggests that this sensitivity may be even less [33]. This was found by Greiner and Derler [4] in short cylinders which were most sensitive to eigenmode imperfections and by Pircher [7] who found that a weld depression is the most detrimental at intermediate lengths. Given the complexity of behaviour in different regimes identified above, and the large range of potential imperfection forms to be examined [12], this paper presents only a small sample that explores eigenmode and nonlinear incremental buckling mode imperfections in cylinders with $r/t = 500$. The nonlinear incremental mode is found by comparing two adjacent displaced shapes at the point of instability (whether limit point or bifurcation) in a geometrically nonlinear analysis.

A reference imperfection amplitude was determined according to the rules in EN 1993-1-6 [12] and ECCS EDR5 [10] for dimple tolerances based on gauge measurements. The dimple amplitude $\Delta w_{0\theta;}$ is assessed in terms of the dimple parameter $U_{0\theta}$ given by

$$U_{0\theta} = \Delta w_{0\theta}/\ell_{g\theta} \tag{8}$$

where gauge length $\ell_{g\theta}$ is given by [10,12]:

$$\ell_{g\theta} = 2.3(\ell/r)^{1/2}(t/r)^{1/4}r, \quad \text{but } \ell_{g\theta} \leqslant r \tag{9}$$

The measured value of $U_{0\theta}$ should meet $U_{0\theta} \leqslant U_{0,\max}$, where $U_{0,\max}$ is the dimple tolerance parameter for a chosen fabrication tolerance quality class. The reference value was chosen here to take the value $U_{0\theta} = U_{0,\max} = 0.01$ corresponding to "High" quality.

7.2. Buckling strength predictions ($r/t = 500$)

Load–deflection curves for stocky cylinders ($L/r = 3$) with eigenmode imperfections are shown in Fig. 18 using a range of imperfection amplitudes relative to the reference value $\Delta w_{0\theta}$ derived from Eqs. (8) and (9). At low amplitudes, a limit load is passed, followed by a bifurcation, leading to a clear definition of strength. However, above 80% of the reference value, the limit load disappears and failure is difficult to define, except as an inflection point on the curve, as suggested by Yamaki [28].

The corresponding information for an intermediate length ($L/r = 7$) with an imperfection in the nonlinear incremental mode

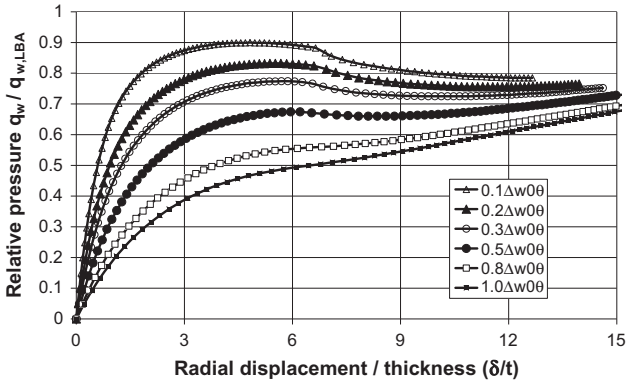

Fig. 18. Nonlinear load–deflection curves for stocky cylinders with a linear eigenmode imperfection ($L/r = 3$, $r/t = 500$).

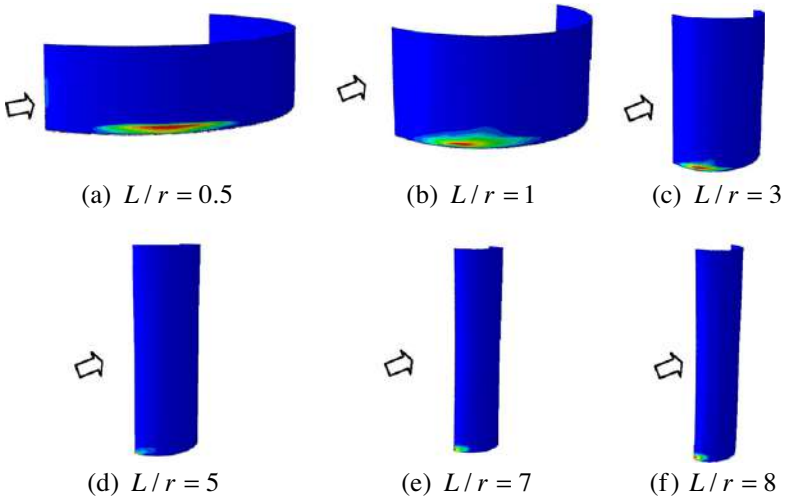

Fig. 17. Zones of plasticity at the nonlinear buckling pressure for cylinders with different L/r under wind pressure ($r/t = 200$).

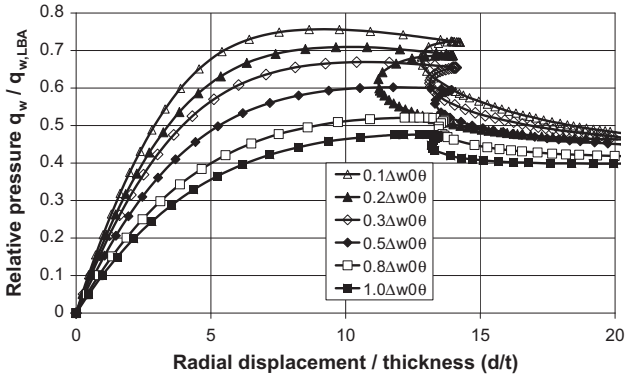

Fig. 19. Nonlinear load–deflection curves for intermediate cylinders with a nonlinear incremental buckling mode imperfection ($L/r = 7$, $r/t = 500$).

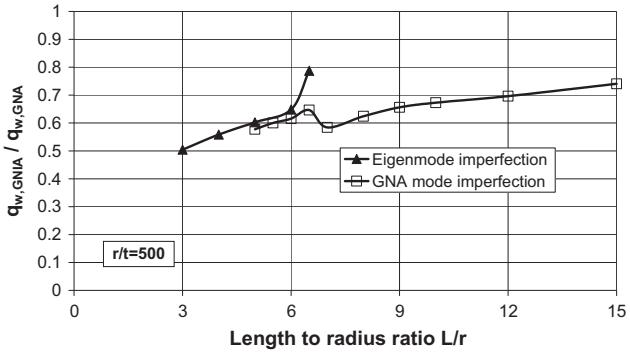

Fig. 21. Strength loss due to reference amplitude imperfections for different L/r and different imperfection forms.

is shown in Fig. 19. The limit load is now sustained at large amplitude imperfections and is followed by a stronger bifurcation with abrupt loss of strength.

Imperfection sensitivity curves derived from these two figures, representing the fall in strength below the geometrically nonlinear value for the perfect structure, are shown in Fig. 20, where the stocky cylinder (cf. Fig. 15) with $L/r = 3$ has linear eigenmode imperfections whilst the intermediate cylinder (cf. Fig. 15) with $L/r = 7$ has nonlinear incremental imperfections.

The simplicity of these curves makes them easy to represent with functions previously used for buckling under axial compression [34,35] in the form

$$\alpha_{imp} = \frac{q_{wGNIA}}{q_{wGNA}} = \frac{1}{1 + a(\Delta_w/\Delta_{w\theta 0})^b} \tag{10}$$

which permits a range of curves to be simply captured. Here, $b = 1$ represents both curves well, with $a = 0.963$ and 0.716 for $L/r = 3$ and 7 respectively as shown by the dashed lines in Fig. 20. This form of curve permits the different fabrication qualities of EN 1993-1-6 [12] to be addressed. The only additional information required to generalise this concept is the calibrating magnitude of the imperfect buckling pressure for the reference imperfection magnitude for different conditions. A sample of such results is shown in Fig. 21, presenting the strength ratio $q_{w,GNIA}/q_{w,GNA}$ which indicates the reduction in strength caused by imperfections below the geometrically nonlinear value shown in Fig. 14. The result indicates that imperfections play a stronger role in stocky cylinders than in intermediate cylinders, but a fuller exploration of the problem is required to complete this description.

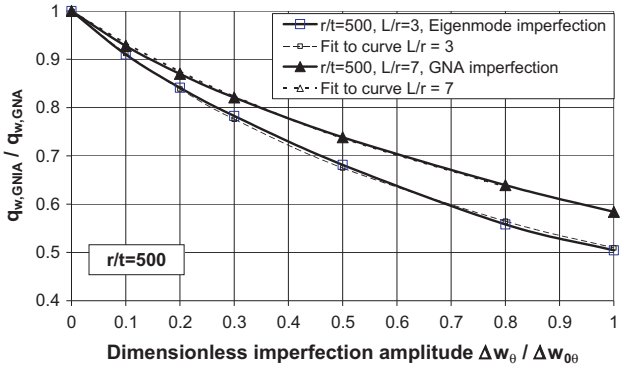

Fig. 20. Imperfection sensitivity curves for two values of L/r with different imperfection forms.

A more comprehensive exploration of the imperfection sensitivity variation with the geometric parameters is beyond the scope of this paper, but the above lays the foundations for a complete description of the imperfect buckling strength of wind loaded cylinders.

8. Conclusions

The complex buckling behaviour of silos and anchored tanks of practical geometry under wind pressure has been studied in this paper. Both the linear (LBA) and nonlinear (GNA) buckling behaviour were explored for a wide range of the geometric parameters.

The categories of stocky, intermediate and slender cylinders have been redefined, and it has been shown that different dimensionless length parameters control the linear buckling and nonlinear buckling strengths. It has also been shown that the concept of relating the wind buckling stagnation pressure to the uniform external buckling pressure is only useful if the simple Donnell theory reference pressure is used.

Expressions usable in design calculations have been developed which permit a comprehensive and accurate treatment of wind buckling through the linear bifurcation pressure and the effects of geometric nonlinearity on the perfect structure. The effects of geometric imperfections of different amplitudes and forms, together with those of plasticity have been investigated. Plasticity evidently has no macroscopic effect on the buckling strength in cylinders with $r/t \geqslant 500$, but is detrimental in thicker cylinders.

References

[1] Resinger F, Greiner R. Kreiszylinderschalen unter Winddruck — Anwendung auf die Beulberechnung oberirdischer Tankbauwerke. Stahlbau 1981;50:65–72.
[2] Resinger F, Greiner R. Buckling of wind-loaded cylindrical shells – application to unstiffened and ring-stiffened tanks. In: Ramm E, editor. Buckling of shells. Berlin: Springer-Verlag; 1982. p. 305–32.
[3] Ansourian P. Stability under wind loading. In: Rotter JM, editor. Design of steel bins for the storage of bulk solids. Sydney: Univ. of Sydney; 1985. p. 138–43.
[4] Greiner R, Derler P. Effect of imperfections on wind-loaded cylindrical shells. Thin-Walled Struct 1995;23:271–81.
[5] Greiner R. Cylindrical shells: wind pressure. In: Brown CJ, Nielsen J, editors. SILOS – fundamentals of theory, behaviour and design. London: E&FN Spon; 1998. p. 378–414.
[6] Greiner R, Guggenberger W. Tall cylindrical shells under wind pressure. In: Teng JG, Rotter JM, editors. Buckling of thin metal shells. London: Spon; 2004. p. 198–206.
[7] Pircher M. Medium-length thin-walled cylinder under wind loading – case study. J Struct Eng 2004;130(12):2062–9.
[8] Jaca RC, Godoy LA, Flores FG, Croll JGA. A reduced stiffness approach for the buckling of open cylindrical tanks under wind loads. Thin-Walled Struct 2007;45:727–36.
[9] Schneider W, Zahlten W. Load-bearing behaviour and structural analysis of slender ring-stiffened cylindrical shells under quasi-static wind load. J Constr Steel Res 2004;60:125–46.

[10] Rotter JM, Schmidt H. European recommendations for steel construction: buckling of shells, 5th ed. Brussels: European Convention for Constructional Steelwork; 2008.
[11] Greiner R, Guggenberger W, Schneider W. Cylindrical shells and wind loading. In: Rotter JM, Schmidt H, editors. Stability of steel shells: European design recommendations. Brussels: European Convention for Constructional Steelwork; 2008. p. 237–58.
[12] EN 1993-1-6 Eurocode 3: design of steel structures, Part 1.6: Strength and stability of shell structures. Brussels: CEN; 2007.
[13] Schnell W. Einfluss der Randverwölbung auf die Beulwerte von Zylinderschalen unter Manteldruck. Stahlbau 1965;34:187–90.
[14] MacDonald PA. Wind loads on circular cross-section bins, silos and tanks. M. Eng. Sci. Thesis. Sydney: Univ. Sydney; 1987.
[15] MacDonald PA, Kwok KCS, Holmes JD. Wind loads on circular storage bins, silos and tanks: I. Point pressure measurements on isolated structures. J Wind Eng Ind Aerodynam 1988;31:165–88.
[16] Rotter JM. Wind pressure distributions on squat silos and tanks. Research Report R01-02. Institute for Infrastructure and Environment, Univ. of Edinburgh; 2001.
[17] EN 1993-4-1 Eurocode 3: Design of steel structures, Part4.1: Design of steel structures: Silos. Brussels: CEN; 2007.
[18] Hibbitt, Karlsson and Sorensen. ABAQUS User's Manual Ver 6.2. Rhode Island: USA: Hibbit, Karlsson and Sorensen Inc. Pawtucket; 2002.
[19] Schneider W. Bemessung der Ringsteifen stählerner Kamine. Stahlbau 2002;71:670–7 [in German].
[20] Chen L, Rotter JM, Doerich C. Buckling behaviour of cylindrical shells of stepwise wall thickness under uniform external pressure. Eng Struct 2011;33(12):3570–8.
[21] Rotter JM. Shell buckling and collapse analysis for structural design: the new framework of the European standard. In: Drew HR, Pellegrino S, editors. New approaches to structural mechanics, shells & biological struts. London: Kluwer Academic; 2002. p. 355–78.
[22] Rotter JM. The practical design of shell structures exploiting different methods of analysis. In: Proc., the 8th conference on shell structures: theory and applications. Gdańsk-Jurata, Poland: Kluwer; 2005. p. 71–86.
[23] Sadowski AJ, Rotter JM. Study of buckling in steel silos under eccentric discharge flows of stored solids. J Eng Mech, ASCE 2010;136(6):769–76.
[24] Batdorf SB. A simplified method of elastic stability analysis for thin cylindrical shells. NACA TN 1947; No. 1341.
[25] Ebner H. Theoretical and experimental investigations on buckling of cylindrical tanks subjected to reduced pressure. Stahlbau 1952;21:153–9.
[26] Brendel B, Ramm E, Fischer DF, Rammerstorfer FG. Linear and non-linear stability analysis of thin cylindrical shells under wind loads. J Struct Mech 1981;9(1):91–113.
[27] Donnell LH. Beams, plates and shells. New York: McGraw Hill; 1976.
[28] Yamaki N. Elastic stability of circular cylindrical shells. Amsterdam, North Holland: Elsevier Applied Science Publishers; 1984.
[29] Holst JMFG, Rotter JM. Axially compressed cylindrical shells with local settlement. Thin-Walled Struct 2005;43(5):811–25.
[30] Doerich C, Rotter JM. Behavior of cylindrical steel shells supported on local brackets. J Struct Eng, ASCE 2008;134(8):1269–77.
[31] Calladine CR. Theory of shell structures. Cambridge: Cambridge University Press; 1983.
[32] Schneider W, Timmel I, Höhn K. The conception of quasi-collapse-affine imperfections – a new approach to unfavourable imperfections of thin-walled shell structures. Thin-Walled Struct 2005;43(8):1202–24.
[33] Rotter JM, Cai M, Holst JMFG. Buckling of thin cylindrical shells under locally elevated axial compression stresses. J Press Vess Technol 2011;133(1): 011204-1–011204-11.
[34] Rotter JM. The elastic–plastic imperfection sensitivity of axially compressed cylinders with weld depressions. In: Graz, Austria: Proc., Eurosteel 2008 conference; 2005. p. 1497–502.
[35] Chen L, Doerich C, Rotter JM. A study of cylindrical shells under global bending in the elastic–plastic range. Steel construction – design and research. Stahlbau 2008;1(1):59–65.